Title

Clinical significance and molecular annotation of cellular morphometric subtypes in lower-grade gliomas discovered by machine learning

Journal

Neuro-Oncology, 25(1)

ISSN

1522-8517

Authors

Liu, Xiao-Ping
Jin, Xiaoqing
Ahmadian, Saman Seyed
et al.

Publication Date

2023-01-05

DOI

10.1093/neuonc/noac154

Peer reviewed

Neuro-Oncology
25(1), 68–81, 2023 | https://doi.org/10.1093/neuonc/noac154 | Advance Access date 18 June 2022

Clinical significance and molecular annotation of cellular morphometric subtypes in lower-grade gliomas discovered by machine learning

Xiao-Ping Liu[†], Xiaoqing Jin[†], Saman Seyed Ahmadian, Xu Yang, Su-Fang Tian, Yu-Xiang Cai, Kuldeep Chawla, Antoine M. Snijders, Yankai Xia, Paul J. van Diest, William A. Weiss, Jian-Hua Mao, Zhi-Qiang Li[‡], Hannes Vogel[‡], and Hang Chang[‡]

Biological Systems and Engineering Division, Lawrence Berkeley National Laboratory, Berkeley, California, USA (X.P.L., X.J., X.Y., A.M.S., J.H.M., H.C.); Berkeley Biomedical Data Science Center, Lawrence Berkeley National Laboratory, Berkeley, California, USA (X.P.L., X.J., X.Y., K.C., A.M.S., J.H.M., H.C.); Department of Emergency, Zhongnan Hospital of Wuhan University, Wuhan, Hubei, China (X.J.); Department of Pathology, Stanford University Medical Center, Stanford, California, USA (S.S.A., H.V.); Key Laboratory of Modern Toxicology of Ministry of Education, School of Public Health, Nanjing Medical University, Nanjing, Jiangsu, China (X.Y., Y.X.); Department of Pathology, Zhongnan Hospital of Wuhan University, Wuhan, Hubei, China (S.F.T., Y.X.C.); Department of Pathology, University Medical Center Utrecht, Utrecht, The Netherlands (P.J.D.); Departments of Neurology, Neurological Surgery, and Pediatrics, University of California, San Francisco, San Francisco, California, USA (W.A.W.); Department of Neurosurgery, Zhongnan Hospital of Wuhan University, Wuhan, Hubei, China (Z.Q.L.)

[†]Equally contributed first authors.
[‡]Equally contributed senior authors.

Corresponding Authors: Zhi-Qiang Li, MD, PhD, Department of Neurosurgery, Zhongnan Hospital of Wuhan University, 169 East Lake Road, Wuchang District, Wuhan, Hubei 430071 China (lizhiqiang@znhospital.cn); Hang Chang, PhD, Biological Systems and Engineering Division, Lawrence Berkeley National Laboratory, 1 Cyclotron Road, Berkeley, CA 94720, USA (hchang@lbl.gov).

Abstract

Background. Lower-grade gliomas (LGG) are heterogeneous diseases by clinical, histological, and molecular criteria. We aimed to personalize the diagnosis and therapy of LGG patients by developing and validating robust cellular morphometric subtypes (CMS) and to uncover the molecular signatures underlying these subtypes.

Methods. Cellular morphometric biomarkers (CMBs) were identified with artificial intelligence technique from TCGA-LGG cohort. Consensus clustering was used to define CMS. Survival analysis was performed to assess the clinical impact of CMBs and CMS. A nomogram was constructed to predict 3- and 5-year overall survival (OS) of LGG patients. Tumor mutational burden (TMB) and immune cell infiltration between subtypes were analyzed using the Mann-Whitney *U* test. The double-blinded validation for important immunotherapy-related biomarkers was executed using immunohistochemistry (IHC).

Results. We developed a machine learning (ML) pipeline to extract CMBs from whole-slide images of tissue histology; identifying and externally validating robust CMS of LGGs in multicenter cohorts. The subtypes had independent predicted OS across all three independent cohorts. In the TCGA-LGG cohort, patients within the poor-prognosis subtype responded poorly to primary and follow-up therapies. LGGs within the poor-prognosis subtype were characterized by high mutational burden, high frequencies of copy number alterations, and high levels of tumor-infiltrating lymphocytes and immune checkpoint genes. Higher levels of PD-1/PD-L1/CTLA-4 were confirmed by IHC staining. In addition, the subtypes learned from LGG demonstrate translational impact on glioblastoma (GBM).

Conclusions. We developed and validated a framework (CMS-ML) for CMS discovery in LGG associated with specific molecular alterations, immune microenvironment, prognosis, and treatment response.

Key Points

- CMS-ML discovers robust CMS in LGG and enables accurate patient stratification.
- CMSs are significantly associated with clinical outcomes.
- CMSs are significantly associated with specific molecular alterations and immune microenvironment.

Graphical Abstract

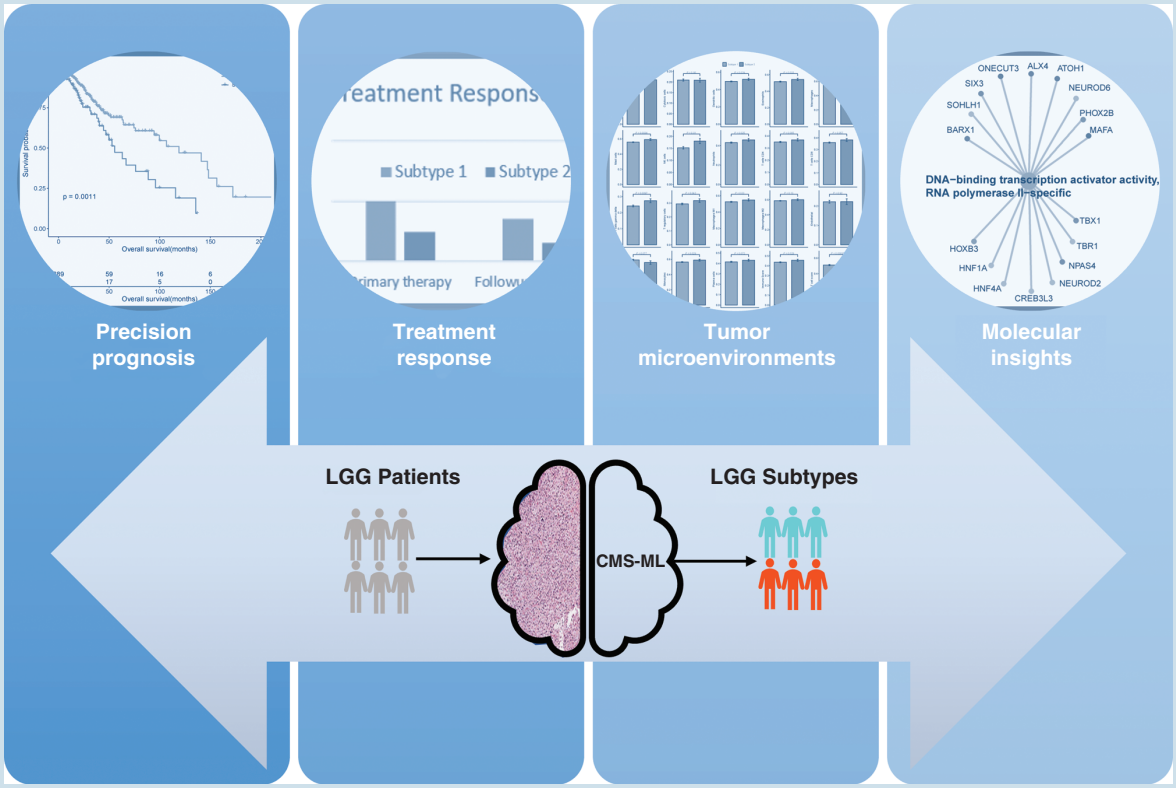

Importance of the Study

LGGs are highly heterogeneous both at the histopathological and molecular level reflected in significant variability in clinical outcomes. Therefore, to personalize care and treatment of LGG patients, accurate and robust patient stratification, which is significantly associated with clinical outcomes, is mandatory. In this study, we developed and multicentrically validated a framework (CMS-ML) for CMS discovery in LGG associated with specific molecular alterations, immune microenvironment, prognosis, and treatment response. And the subtypes learned from LGG demonstrate translational impact on glioblastoma. Our findings have potential clinical implications to facilitate precision diagnosis and personalized treatment of LGG patients. In addition, CMS-ML may provide potential clinical value across tumor types.

Gliomas is the most common primary central nervous system (CNS) malignant tumor, accounting for ~80% of all CNS malignancies.[1] According to the 2007 WHO classification, gliomas were categorized into grades 1-4.[2] The 2021 WHO classification[3] introduced a paradigm shift in the classification of CNS tumors combining histopathologic and genotypic features[4] to reveal an "integrated" diagnosis. Factors affecting overall survival (OS) include age >40 years, astrocytic subtype, tumor maximum diameter >6 cm, tumors crossing the midline, and the patient's degree of neurological impairment, Karnofsky performance score, multiple lesions, IDH-mutant status, 1p19q status, TERT mutation status, and ATRX mutation status.[5–8] Moreover, lower-grade gliomas (LGGs) are highly

heterogeneous both at histopathological and molecular levels,[4,9] resulting in significant variability in clinical outcomes.[9,10] Therefore, to personalize care and treatment of LGG patients, accurate and robust patient stratification, which is significantly associated with clinical outcomes, is mandatory.

Cellular morphometric properties play key roles in cancer diagnosis and prognosis together with important molecular factors. Recently, deep neural networks (eg, convolutional neural network [CNN]) have been successfully applied in several glioma-related studies.[11–13] However, the quantitative profiling and molecular association of the cellular morphometric landscape from whole-slide images (WSIs) remain inadequately investigated due to both technical and conceptual limitations.

To capture the heterogeneous cytoarchitecture of gliomas, we developed a high-throughput and robust computational pipeline that quantifies tissue histology at the cellular level[14] with applications to tumor classification[15] and molecular association.[16] In addition, we introduced stacked predictive sparse decomposition (SPSD)[17] for mining underlying cellular morphometric properties within WSI. Here, we applied SPSD to LGG cohorts to discover clinically relevant cellular morphometric subtypes (CMSs) and evaluate the clinical impacts and molecular correlation of CMSs.

Methods

Data Collection

The patient data in this retrospective study, including tissue histology diagnostic slides and the clinical information, were collected from TCGA-LGG cohort (Supplementary Table 1), Zhongnan Hospital of Wuhan University (ZN-LGG cohort, between January 2016 and May 2019, Supplementary Table 2), the Medical Center of Stanford University (SU-LGG cohort, between January 2013 and December 2014, Supplementary Table 3), TCGA-GBM cohort (Supplementary Table 4), and Zhongnan Hospital of Wuhan University (ZN-GBM cohort, between January 2016 and May 2019, Supplementary Table 5) to form the discovery cohort and multicenter validation cohorts. The inclusion criteria were primary LGG and GBM with diagnostic slides and OS information available. This study was approved by the institutional review board (IRB) of Zhongnan Hospital of Wuhan University, Stanford University, and Lawrence Berkeley National Laboratory, with a waiver of informed consent.

Treatment Response in TCGA-LGG Cohort

The treatment response in TCGA-LGG cohort was assessed using Response Evaluation Criteria in Solid Tumors (RECIST)[18] as complete remission, partial remission, progressive disease, and stable disease. Here, we categorized patient response into Response (including complete/partial remission), and non-Response (including progressive/stable disease).

Identification of Cellular Morphometric Biomarkers

We developed an unsupervised machine learning pipeline based on SPSD[17] for the discovery of underlying cellular morphometric characteristics from the 15 cellular morphometric features extracted from the WSIs of TCGA-LGG cohort (Supplementary Method 1). We then identified 256 cellular morphometric biomarkers (CMBs) for cellular object representation. Specifically, we used a single network layer with 256 dictionary elements (ie, CMBs) and sparsity constraint 30 at a fixed random sampling rate of 1000 cellular objects per WSI from TCGA-LGG cohort (Supplementary Figure 2A), where the network parameters (ie, dictionary size and sparsity) were experimentally optimized to maintain the data reconstruction error ratio under certain threshold (ie, 10% in this study, Supplementary Figure 2B and C). The pre-trained SPSD model reconstructed each cellular object as a sparse combination of pre-identified 256 CMBs, and thereafter represented it as the sparse code (ie, reconstruction sparse coefficients), where the sparsity constraint enforced the reconstruction contribution mainly from the top 30 CMBs.

Clinical and Biological Evaluation of CMBs

We evaluated the prognostic impact of the top 30 CMBs with largest variations mined from TCGA-LGG cohort with Cox proportional hazards regression (CoxPH) model (survival package in R, Version 3.2-3), and examined the effects of high or low levels of each prognostic significant CMB on OS using Kaplan-Meier analysis (survminer package in R, Version 0.4.8) and log-rank test (survival package in R, Version 3.2-3), where TCGA-LGG cohort was divided into CMB-high and CMB-low groups per CMB (survminer package in R, Version 0.4.8). Meanwhile, we evaluated biological significance between these groups by assessing their relationship with factors available in TCGA-LGG cohort using the Mann-Whitney *U* test.

Construction of Patient-level Cellular Morphometric Context Representation

The patient-level representation was constructed based on pre-identified 256 CMBs as an aggregation (ie, max-pooling) of all the cellular sparse codes extracted via pre-built SPSD model from the cellular objects belonging to the same patients following these steps consecutively: (1) delineation of cellular architecture and extraction of cellular morphometric properties from WSIs of each patient; (2) construction of cellular sparse codes for the cellular objects belonging to each patient based on pre-identified 256 CMBs and pre-built SPSD model; (3) aggregation (ie, max-pooling) of all cellular sparse codes belonging to the same patient to form the patient-level cellular morphometric representation; and (4) selection of the top 30 CMBs with the largest variations identified in TCGA-LGG cohort as the final patient-level cellular morphometric representation.

Identification and Application of CMS

The CMS was identified based on patient-level cellular morphometric context representation through consensus clustering[19] (ConsensusClusterPlus R package, Version 1.50.0) with hierarchical clustering, Pearson's correlation, and 500 bootstrapping iterations; and the optimal number of subtypes was determined by the consistency of cluster assignment (consensus matrix) and the prognostic impact of subtypes. For a new patient, the subtype was assigned as follows: (1) construct patient-level cellular morphometric context representation with pre-built CMBs and SPSD model; (2) calculate the Pearson's distances between the new patient's representation and the mean representation of each pre-identified patient subtype; and (3) assign the new patient to its closest subtype yielding smallest Pearson's distance.

Clinical Evaluation and Validation of CMS

We evaluated and independently validated the clinical impact of pre-identified CMSs from TCGA-LGG cohort, ZN-LGG cohort, SU-LGG cohort, TCGA-GBM cohort, and ZN-GBM cohort, respectively. Refer to Supplementary Method 2 for details.

Differences in Gene Expression, Mutation Load, and Immune Microenvironment Between CMSs

We evaluated the differences in gene expression, mutation load, and immune microenvironment between CMSs. Refer to Supplementary Methods 3 for details.

Immunohistochemistry Staining

Immunohistochemistry (IHC) staining was carried out on 4-μm sections of formalin-fixed and paraffin-embedded tissues according to standard protocols (see Supplementary Method 4 for details).

Statistical Analysis

Refer to Supplementary Method 5 for details.

Results

Study Design and Characteristics of Patient Cohorts

We used three retrospective LGG cohorts to evaluate and independently validate the prognostic impact of CMSs; and used two retrospective GBM cohorts to evaluate the generalizability and translational impact of LGG-driven CMSs in GBM (Figure 1). The TCGA-LGG cohort served as discovery set including 488 LGG patients. There were 271 (55.5%) male and 217 (44.5%) female patients, with a median age of 41 years (range: 14-87 years). The ZN-LGG cohort included 70 LGG patients, where 36 patients (51.4%) were male and 34 (48.6%) were female. Median age was 47.0 years (range: 6-72 years). The SU-LGG cohort included 37 LGG patients, where 22 patients (59.5%) were male and 15 (40.5%) were female, and the median age was 41.0 years (range: 1-83 years). The TCGA-GBM cohort included 380 GBM patients, where 145 patients (38.2%) were male and 234 (61.6%) were female and the median age was 59.0 years (range: 10-89 years). The ZN-GBM cohort included 77 GBM patients, where 23 patients (29.9%) were male and 53 (68.8%) were female and the median age was 56.0 years (range: 5-81 years).

Identification of CMBs Using Unsupervised Representation Learning

Our pipeline[14] recognized and delineated over 400 million cellular objects from TCGA-LGG chort; over 25 million cellular objects from ZN-LGG cohort; over 10 million cellular objects from SU-LGG cohort; over 400 million cellular objects from TCGA-GBM cohort; and over 25 million cellular objects from ZN-GBM cohort, where each cellular object was represented with 15 morphometric properties (Supplementary Figure 1A, Supplementary Table 6, Supplementary Method 1).

Next, we trained SPSD[17] model based on pre-quantified cellular objects randomly selected from TCGA-LGG cohort to discover the CMBs (Supplementary Figure 2). After training, the pre-built SPSD model reconstructed each cellular object as a sparse combination of the pre-identified 256 CMBs, which led to the novel representation of each single cellular object as the 256 sparse codes. Thereafter, the corresponding 256-dimensional cellular morphometric context representation of each patient was an aggregation (Supplementary Figure 1B) of all delineated cellular objects belonging to that patient (Supplementary Tables 7–11). The final patient-level cellular morphometric context representation was optimized by using the top 30 CMBs with the largest variations (sparsity constraint of SPSD model), which contributed to 98.84% of the total data variations.

Clinical and Biological Evaluation of CMBs

We next evaluated the association of the 30 CMBs with respect to histological meanings, prognosis, and cancer biology. Our survival analysis revealed that 20 CMBs had significant prognostic impact (false discovery rate [FDR] < 0.05), where 5 of them were prognostically favorable (hazard ratio [HR] < 1) and 15 prognostically unfavorable (HR > 1) (Figure 2A, Supplementary Figure 3, Supplementary Table 12). Examples of prognostically significant CMBs (Figure 2A, Supplementary Figure 3) demonstrated the capability of our pipeline in acquiring biomedically meaningful and interpretable histopathological cellular concepts (Supplementary Table 13). For example, these CMBs captured atypical nuclear contour (eg, CMB_139, CMB_115, CMB_152, CMB_131), nuclear pleomorphism with increasing variation in nuclear size, shape (eg, CMB_208) or multinucleated tumor cells (eg, CMB_145), etc.

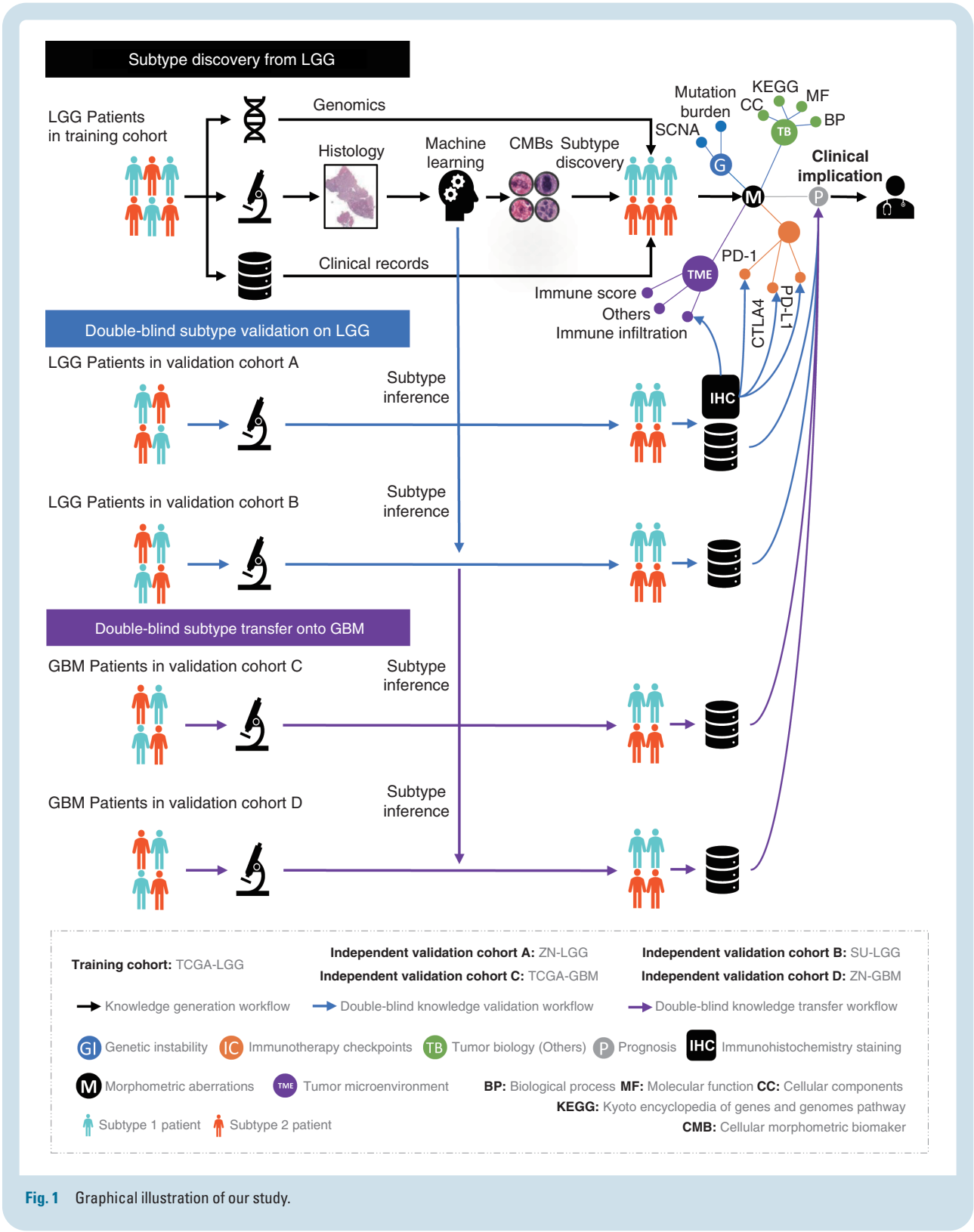

Fig. 1 Graphical illustration of our study.

Additionally, the TCGA-LGG patient cohort was divided into two groups based on each CMB. The Kaplan-Meier curves showed significant impact ($P < .01$, Figure 2B, Supplementary Figure 4) of the levels of each CMB on OS. Thereafter, we evaluated biological significance between patient groups with high and low CMB levels in the TCGA-LGG cohort and discovered significant correlations ($P < .05$) with tumor microenvironment factors, including the relative abundance of tumor immune cells and fibroblast,[20] and predictors of immunotherapy

response (Figure 2C, Supplementary Figures 5 and 6). Levels of prognostically favorable CMBs correlated negatively, whereas levels of prognostic unfavorable CMBs correlated positively with tumor-infiltrating immune cells and the expression levels of PD-1 and PD-L1, but not to fibroblasts ($P > .05$; Figure 2C, Supplementary Figures 5 and 6). Finally, we detected a significant correlation between focal somatic copy number alteration (SCNA) and tumor mutational burden (TMB) ($P < .05$; Figure 2D).

Identification and Validation of CMS

Consensus cluster analysis using 30 CMBs identified three CMSs from TCGA-LGG cohort with significantly differing prognosis (log-rank $P < .0001$; Supplementary Figure 7). Given the small number of patients (n = 4) in subtype 3, as well as its prognostic similarity to subtype 2 patients, we merged subtypes 3 and 2, and referred this combination as subtype 2 in the rest of this study (Figure 3A). Accordingly, the TCGA-LGG cohort contained 389 subtype 1 and 99 subtype 2 patients. The patient-level cellular morphometric context representation in TCGA-LGG cohort formed significantly distinct clusters ($P = .001$, Figure 3B). Importantly, two CMSs, predicted with pre-built subtype model, were portioned in two validation sets. Specifically, ZN-LGG cohort was stratified into subtype 1 (38 patients) and subtype 2 (32 patients), whereas SU-LGG cohort was stratified into subtype 1 (16 patients) and subtype 2 (21 patients). Moreover, the patient-level representation in both validation cohorts also formed significantly distinct clusters ($P = .001$, Figure 3C and D).

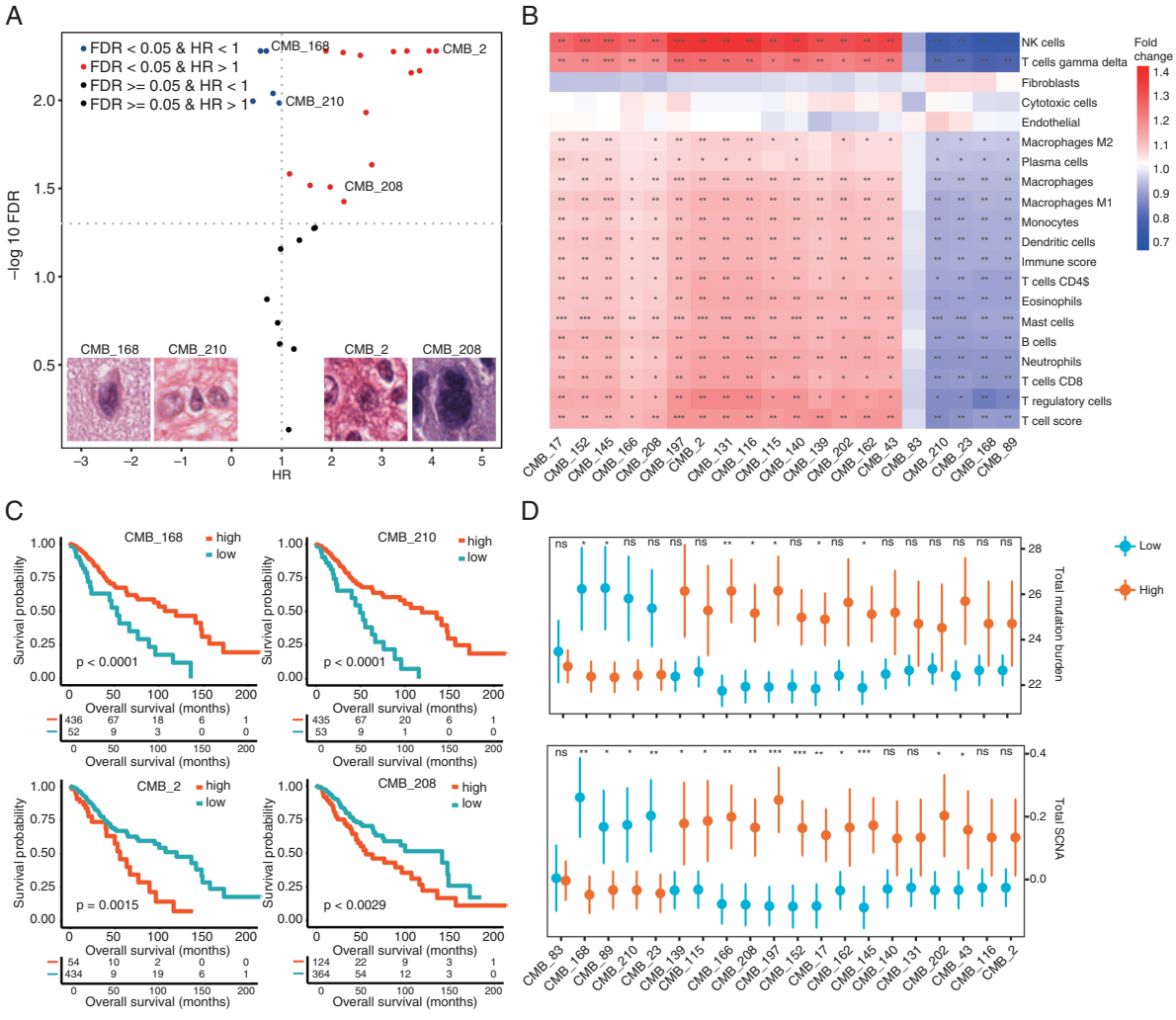

Fig. 2 Unsupervised feature learning discovers CMBs with clinical significance and molecular relevance. (A) Prognostic significant CMBs with favorable and unfavorable examples; (B-D) LGG patients within CMB-low and CMB-high groups show significant differences in various tumor microenvironmental factors (B), overall survival (C), and genetic instability (D).

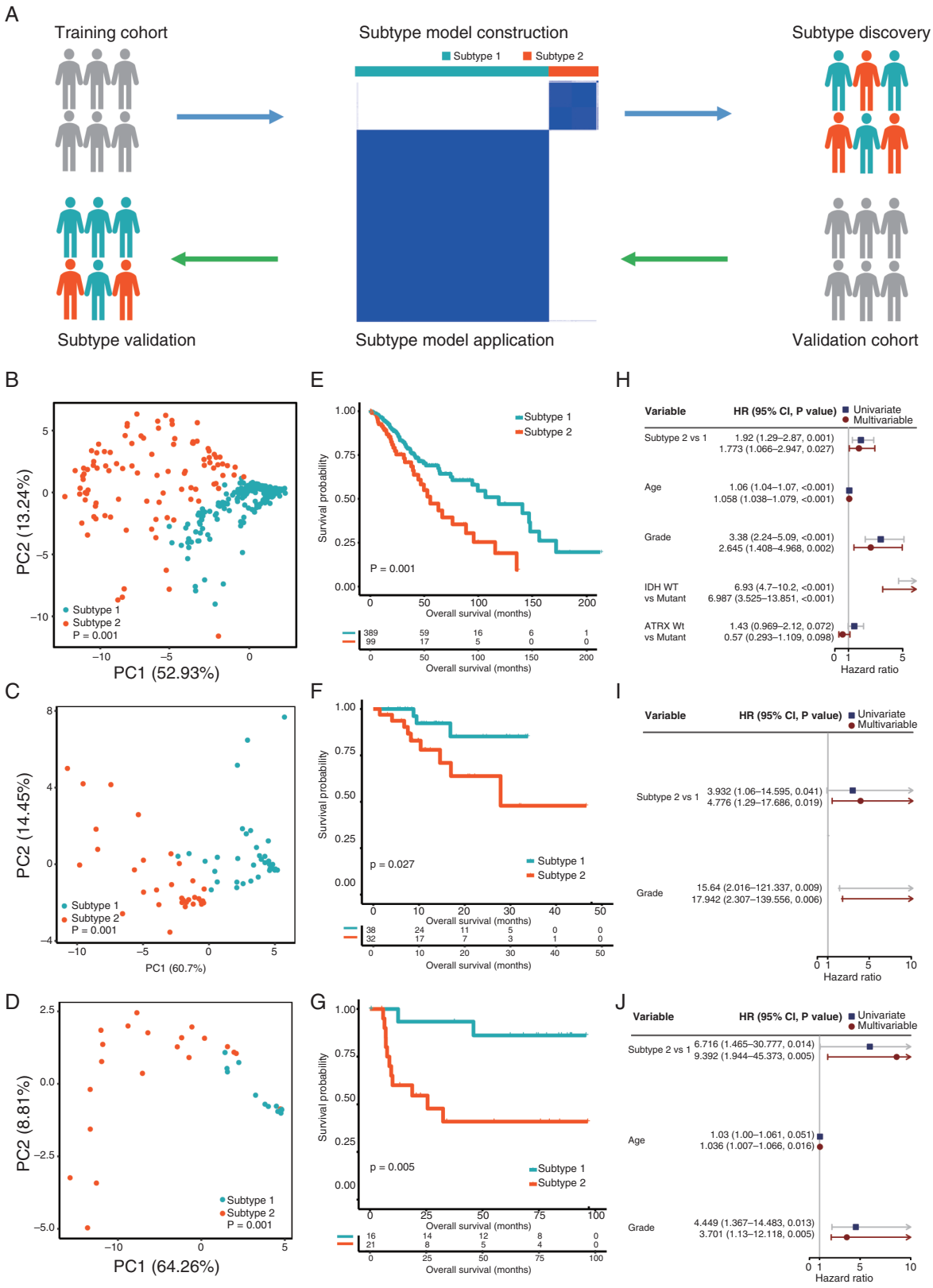

Fig. 3 Lower-grade glioma (LGG) patient subtype provides significant and independent prognostic impact. (A) Consensus clustering model for LGG patient subtypes discovery and inference; (B–D) subtype-specific patients in TCGA-LGG, ZN-LGG, and SU-LGG cohorts form distinct clusters in patient-level cellular morphometric context space; (E–G) subtype-specific patients in TCGA-LGG, ZN-LGG, and SU-LGG cohort show significant difference in survival; (H–J) patient subtype in TCGA-LGG, ZN-LGG, and SU-LGG cohort is a significant and independent prognostic factor.

Clinical Significance of CMSs

We examined the association between CMSs and clinical and tumor characteristics in TCGA-LGG cohort. Surprisingly, there was no significant association between CMSs and any clinical/molecular prognostic factors (including age, grade, histological type, IDH mutation status, 1p/19q codeletion, MGMT promoter status, TERT promoter status, and ATRX status) (Supplementary Table 1). This finding was confirmed in both validation cohorts (Supplementary Tables 2 and 3).

In the TCGA-LGG cohort where genetic alteration burden information was available, Maftool analysis showed significantly higher TMB (P = .003) and focal SCNA score (P = .012) in subtype 2 patients (Supplementary Figure 8), indicating a higher level of genomic instability of tumors from subtype 2.

Kaplan-Meier analysis showed significantly shorter OS of subtype 2 than subtype 1 patients (P = .001, Figure 3E). Furthermore, univariate and multivariate CoxPH models indicated the independent prognostic impact of CMSs in TCGA-LGG cohort after adjusting for other significant clinical and molecular factors, including age, histological type, grade, IDH mutation status, and ATRX mutation status (HR: 1.773, 95% CI: 1.066-2.947, P = .027; Figure 3H, Supplementary Table 14). The combination of CMSs and clinical and molecular factors provided significantly improved (P < .001, Supplementary Figure 9) prediction of OS (median C-index: 0.860, 95% CI: 0.859-0.861) compared to classical models with only clinical and molecular factors (median C-index: 0.857, 95% CI: 0.856-0.858). Moreover, the nomogram (Figure 4A), built upon patient subtype and clinical and molecular factors, significantly correlated with OS of TCGA-LGG patients, and provided excellent prediction [C-indexes for validation on the training set and testing set with 1000 bootstraps were 0.8334 (95% CI: 0.8322-0.8345) and 0.8014 (95% CI: 0.8001-0.8026), respectively] of the 3- and 5-year OS of TCGA-LGG patients, which was further confirmed by calibration analysis on the training (Figure 4B and C) and testing set (Figure 4D and E), respectively. Meanwhile, a dynamic nomogram further facilitated its potential clinical implications at: https://liuxiaoping.shinyapps.io/LGG_nomogram. Additionally, the chi-square test showed significantly poor response of subtype 2 patients with respect to primary therapy (P < .001) and follow-up treatment (P = .002) (Supplementary Table 1).

Importantly, the double-blind deployment of the pre-built CMS model on both validation cohorts with independent survival analysis confirmed the significantly worse OS of subtype 2 patients (P = .027 in ZN-LGG, P = .005 in SU-LGG, Figure 3F and G). Furthermore, univariate and multivariate CoxPH models confirmed the independent prognostic impact of CMSs after adjustment for other significant clinical factors in both validation cohorts (ZN-LGG: HR: 4.776, 95% CI: 1.29-17.686, P = .019; SU-LGG: HR: 9.392, 95% CI: 1.944-45.373, P = .005; Figure 3I and J, Supplementary Tables 15 and 16).

Interestingly, the direct translation of the pre-built CMS model on TCGA-GBM and ZN-GBM cohorts confirmed the clinical impact of CMS learned from LGG on GBM patients (Supplementary Figure 10). Consistent with our observations on LGG cohorts, GBM patients in both cohorts were stratified into distinct clusters (P = .001 in TCGA-GBM; P = .001 in ZN-GBM; Supplementary Figure 10A and B), and the subtype 2 GBM patients demonstrated significantly worse OS compared with subtype 1 GBM patients (P = .00051 in TCGA-GBM; P < .001 in ZN-GBM; Supplementary Figure 10C and D). Furthermore, univariate and multivariate CoxPH models confirmed the independent prognostic impact of CMSs in GBM patients after adjusting for significant clinical/molecular factors in both GBM cohorts (TCGA-GBM—HR: 1.457, 95% CI: 1.002-2.117, P = .049; ZN-GBM—HR: 3.101, 95% CI: 2.006-7.491, P < .001; Supplementary Figure 10E and F, Supplementary Tables 17 and 18). Furthermore, restricted mean survival time (RMST)[21] analysis on both LGG and GBM patients (Supplementary Table 19) suggested the difference in follow-up times across cohorts had no significant influence on the prognostic value of CMS.

Lastly, we performed pooled analysis combing all LGG and GBM patients into Pooled-LGG (595 patients) and Pooled-GBM (457 patients) cohorts, respectively. The pooled analysis confirmed (1) the significantly distinct stratification of patients (Pooled-LGG: P = .001, Supplementary Figure 11A; Pooled-GBM: P = .001, Supplementary Figure 12A); (2) the significantly worse OS of subtype 2 patients (Pooled-LGG: P < .001, Supplementary Figure 11B; Pooled-GBM: P < .001, Supplementary Figure 12B); and (3) the independent prognostic impact of CMSs in both pooled cohorts (Pooled-LGG—HR: 2.315, 95% CI: 1.617-3.315, P < .001, Supplementary Figure 11C, Supplementary Table 20; Pooled-GBM—HR: 1.57, 95% CI: 1.206-2.044, P = .001, Supplementary Figure 12C, Supplementary Table 21). Interestingly, OS difference between LGG subtypes was independent of tumor grade (Grade2: P = .037; Grade3: P < .0001; Supplementary Figure 11D) and histology types (Astrocytoma: P = .0046, Oligodendroglioma: P = .012, Oligoastrocytoma: P = .0013; Supplementary Figure 11E), further demonstrating the independent clinical value of CMSs.

Molecular Annotation Underlying CMSs

To gain insight into molecular differences underlying CMSs, we used available transcriptome data from TCGA-LGG and identified 316 differentially expressed genes (DEGs) between CMSs ($|\log_2 FC| > 1$, P < .001, Supplementary Figure 13A, Supplementary Table 22), where 147 and 169 genes were upregulated and downregulated, respectively, in subtype 2 compared to subtype 1. Gene ontology (GO) functional enrichment analysis of DEGs demonstrated significant enrichment (FDR < 0.05) for biological processes involving hemostasis, keratinization, intermediate filament organization, humoral immune response, regulation of ERK1 and ERK2 cascade, positive regulation of acute inflammatory response (Supplementary Figure 13B, Supplementary Table 23); Cellular component GO terms significantly enriched (FDR < 0.05) in the DEGs included intermediate filament, blood microparticle, cluster of actin-based cell projections, collagen-containing extracellular matrix, and trans-Golgi network transport vesicle (Supplementary Figure 13C, Supplementary Table 24),

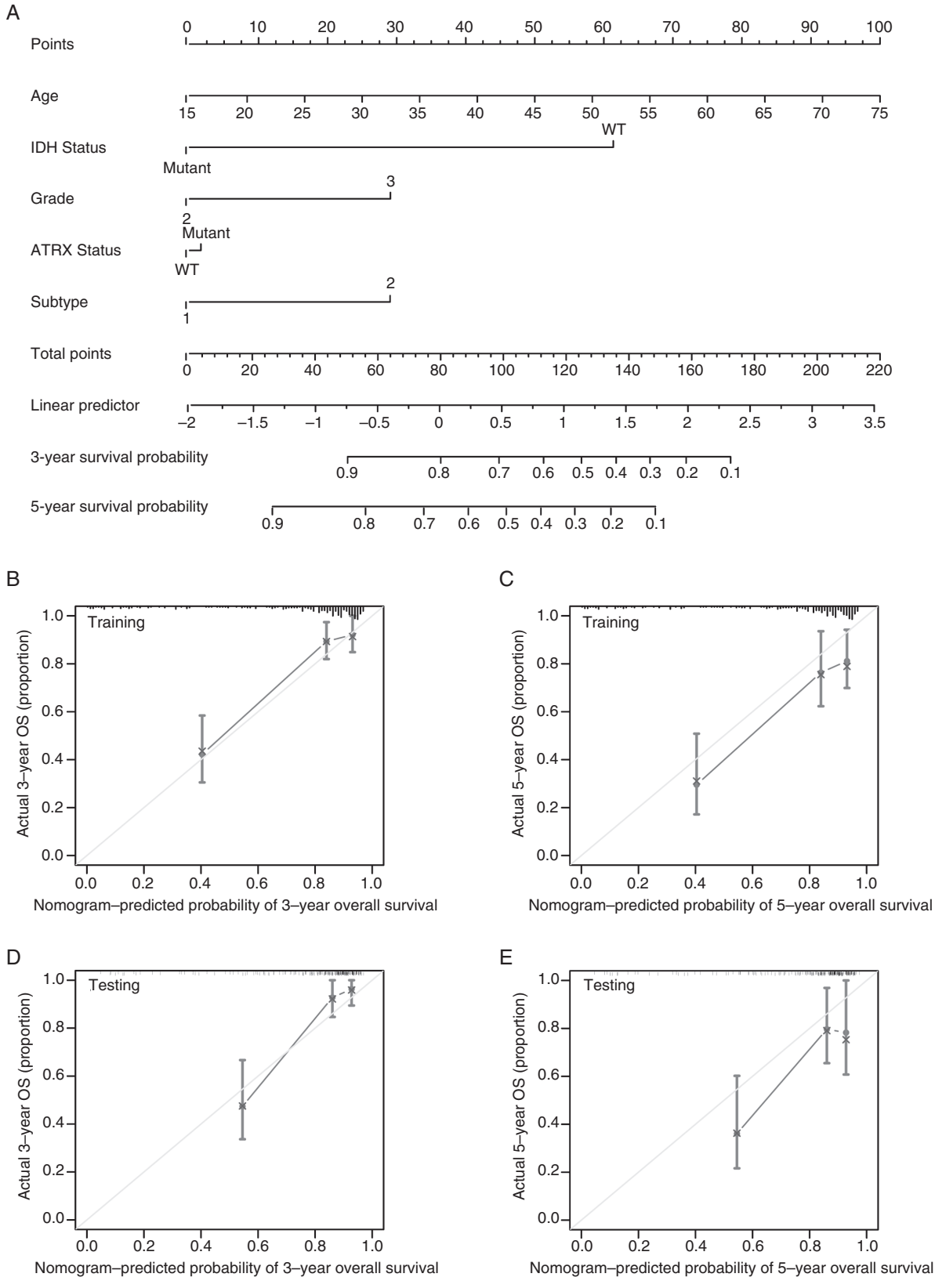

Fig. 4 Development and validation of nomogram predicting the 3- and 5-year survival of lower-grade glioma (LGG) patients. (A) Nomogram predicting the 3- and 5-year survival of LGG patients. (B) Calibration analysis at 3 years in the training set of TCGA-LGG cohort. (C) Calibration analysis at 5 years in the training set of TCGA-LGG cohort. (D) Calibration analysis at 3 years in the test set of TCGA-LGG cohort. (E) Calibration analysis at 5 years in the test set of TCGA-LGG cohort.

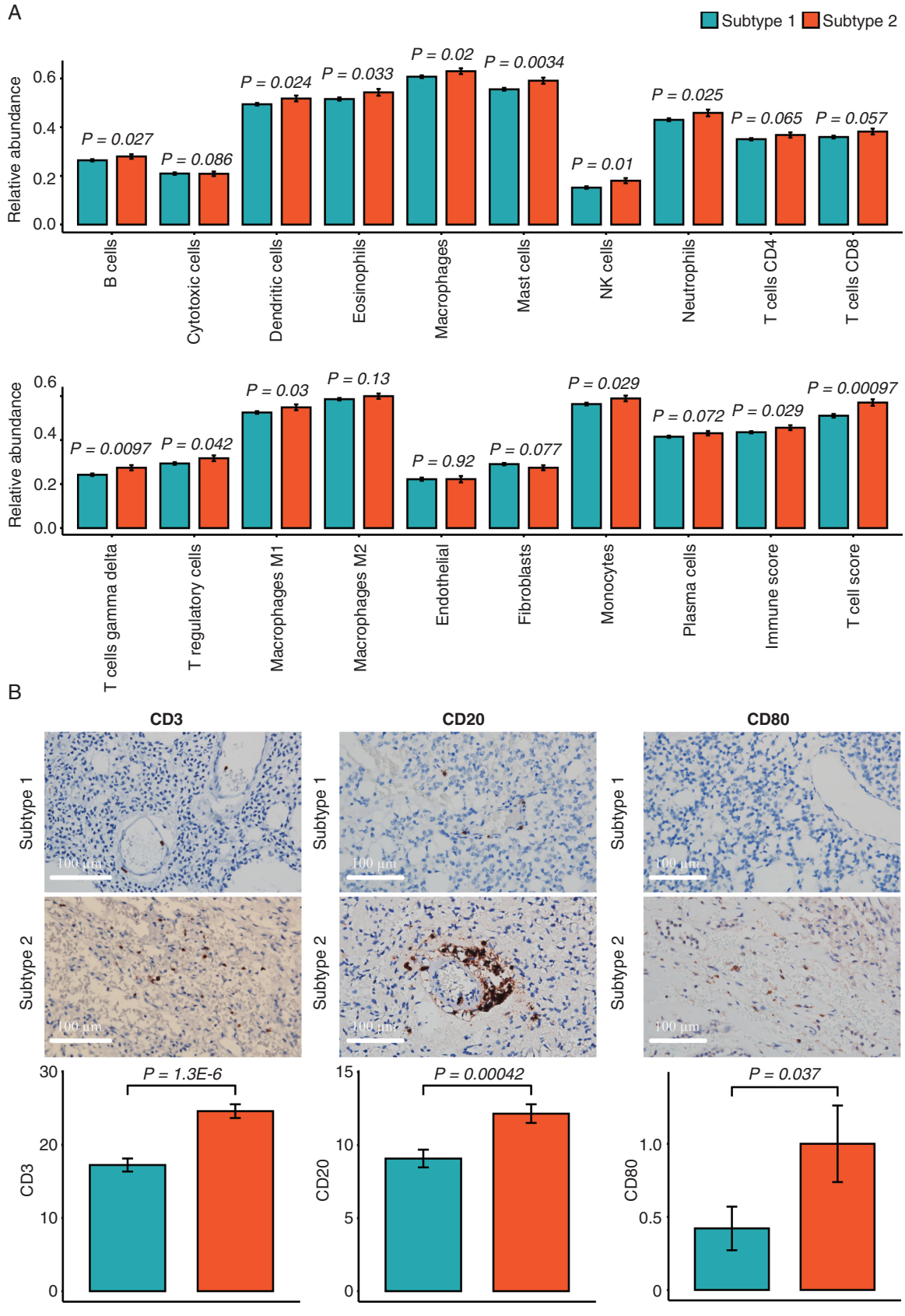

Fig. 5 (A) Patient subtypes in TCGA-LGG cohort show significant difference in various tumor microenvironmental factors. (B) Immunohistochemistry (IHC) staining confirms the significantly more infiltrating T cells ($CD3^+$), B cells ($CD20^+$), and macrophages M1 ($CD80^+$) immune cells in subtype 2 LGG patients (scale bar = 100 μm).

whereas molecular function GO terms (FDR < 0.05) included structural constituent of cytoskeleton and cytokine activity (Supplementary Figure 13D, Supplementary Table 25). KEGG analysis indicated that DEGs were significantly enriched (FDR < 0.05) in neuroactive ligand-receptor interaction, cytokine-cytokine receptor interaction, IL-17 signaling pathway, complement and coagulation cascades, and *Staphylococcus aureus* infection (Supplementary Figure 13E, Supplementary Table 26). Moreover, protein-protein interaction (PPI) network analysis suggested that 72 genes with a degree no less than 5 were at the hub of the network (Supplementary Table 27, Supplementary Figure 14). Together these findings suggest possible differences in the molecular mechanisms of CMSs.

Association of CMSs With Tumor Immune Microenvironment

Based on the molecular annotation of DEGs between CMSs, we investigated their association with the immune microenvironments. Subtype 2 (Figure 5A) showed significantly more infiltrating B cells (P = .027), dendritic cells (P = .024), eosinophils (P = .033), macrophages (P = .02), mast cells (P = .0034), natural killer (NK) cells (P = .01), neutrophils (P = .025), gamma delta T cells (P = .0097), T regulatory cells (P = .0042), macrophages M1 (P = .003), and monocytes (P = .029) compared to subtype 1. There was a trend toward increased abundance of $CD4^+$T cells (P = .065), $CD8^+$ T cells (P = .057), and plasma cells (P = .072) in subtype 2. Moreover, the T-cell infiltration score (P = .00097) and overall immune infiltration score (P = .029) were significantly higher in subtype 2 (Figure 5A). Importantly, we validated the immune infiltrations in the ZN-LGG cohort using IHC (Figure 5B, Supplementary Figure 15), and confirmed the significantly more infiltrating T cells ($CD3^+$) (P = 1.3E-6), B cells ($CD20^+$) (P = .00042), and macrophages M1 ($CD80^+$) (P = .037) in subtype 2 patients. In addition, no statistical difference of macrophages M2 ($CD163^+$) (P = .57) between CMSs was found.

To explore the possibility of immune escape in subtype 2 LGG patients, we examined expression levels of immune suppression molecules CTLA-4, PD-1, the ligand of PD-1 (ie, PD-L1), HAVCR2, LGALS9, CD86, LAG3, PDCD1LG2, CD28, CD96, CD80, and IDO1. In TCGA-LGG (Figure 6A, Supplementary Figure 16), the expression of

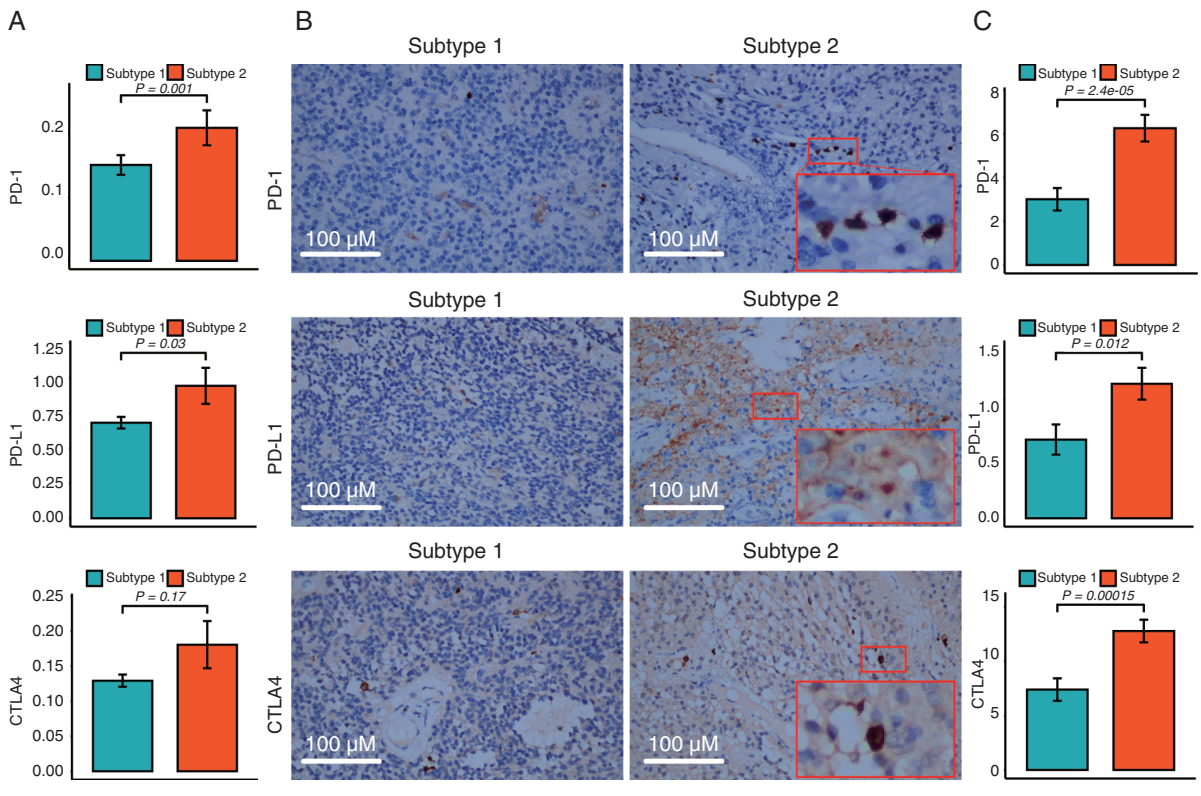

Fig. 6 Immunohistochemistry (IHC) staining confirms the upregulation of PD-1, PD-L1, and CTLA-4 in subtype 2 LGG patients. (A) Subtype-specific expression of PD-1 (first row), PD-L1 (second row), and CTLA-4 (third row) in TCGA-LGG cohort. (B) Representative examples of PD-1 staining (first row), PD-L1 staining (second row), and CTLA-4 staining (third row) in subtype 1 and 2 LGG patients (scale bar = 100 μm), respectively, where PD-1 expression was frequently observed in the plasma of lymphocytes around blood vessels; PD-L1 was widely expressed in the membrane of tumor cells, while slightly in the cytoplasm; and CTLA-4 positive expression was majorly observed in the cytoplasm of lymphocytes around blood vessels. (C) Subtype-specific expression of PD-1 (first row), PD-L1 (second row), and CTLA-4 (third row) was quantified via IHC staining in ZN-LGG cohort.

PD-1 (P = .00044), PD-L1 (P = .03), PDCD1LG2 (P = .014), CD96 (P = .016), CD28(P = .031), CD80 (P = .002), and CD86 (P = .043) were significantly higher in subtype 2 patients, with a similar trend for CTLA-4 (P = .17), TIM3(P = .055), LGALS9 (P = .34), LAG3(P = .14), and IDO1(P = .09). Finally, we validated the expression levels of these immune inhibitory molecular markers in ZN-LGG using IHC and confirmed significant upregulation of PD-1 (P = 8e-05), PD-L1 (P = .018), and CTLA-4 (P = .00089) in subtype 2 (Figure 6B and C). Overall, these results indicated possible mechanisms for immune escape or immune tolerance in subtype 2 tumors, which could explain the poor prognosis of subtype 2 patients and laid the foundation of potential immunotherapy for LGG patients.

Discussion

In this study, we extracted CMBs from WSIs of LGG patients through unsupervised learning strategy and subsequently defined two CMSs. Different from classical biomarkers, the CMBs act as imaging biomarkers capturing the heterogeneity in cellular properties and their microenvironments, which could be further explored as a future direction. The robustness of CMSs was demonstrated in two independent LGG cohorts. Interestingly, although a minority of GBM arises through the progression from LGG, the relevance of CMSs from LGG was shown to have prognostic value in GBM in two independent GBM cohorts, possibly related to common tumor microenvironments between LGG and GBM captured in CMSs. Although the HR of CMS was not as large as the HRs of well-known prognostic factors in gliomas (eg, grade, IDH mutation status), the importance of CMSs lies in its independent prognostic significance after adjusting for other clinical and molecular factors; the relation to immunosuppressive tumor microenvironments; the association with treatment response; and the relation to underlying molecular and phenotypic alterations.

Different from many CNN-like systems, which mainly focus on end-to-end prediction of clinical/molecular endpoints, the emphasis of our study was on novel knowledge discovery with interpretability, robustness, and independent clinical value through multicentric validation. As a further justification, we evaluated a superior CNN-like system (ie, SCNN [survival CNN]), specifically designed and optimized for the prediction of cancer outcomes in brain tumor.[22] Interestingly, the SCNN risk score did not provide independent and significant prognostic value in both TCGA-LGG (P = .182, Supplementary Figure 17A) and TCGA-GBM (P = .533, Supplementary Figure 17B) cohorts, in the presence of CMS and other important clinical/molecular factors, suggesting that CMS out-performed the supervised CNN-like system (ie, SCNN) for precision prognosis.

SCNA score, closely related to the occurrence and progression of many tumors (including glioma), is related to poor prognosis.[23] Meanwhile, TMB levels, closely related to degree of malignancy and poor prognosis of glioma, are often used as a biomarker for predicting the efficacy of anti-PD-1 therapy.[24,25] Our study confirmed significantly higher focal SCNA scores and TMB levels in subtype 2 patients, which explains the poor prognosis and provides justification for anti-PD-1 immunotherapy for subtype 2 patients.

Our KEGG analysis suggested that DEGs were significantly enriched (FDR < 0.05) in neuroactive ligand-receptor interaction, cytokine-cytokine receptor interaction, IL-17 signaling pathway, complement and coagulation cascades, and *S. aureus* infection, which were closely associated with the diagnosis and/or prognosis of glioma.[26–30] Moreover, IL-6, at the hub of the PPI network (Supplementary Figure 14), was recognized as an indicator for the oncogenesis, invasiveness, prognosis, and treatment of patient with glioma.[31–33] In addition, through oncoKB database, we found that MET (mesenchymal-epithelial transition, one of the hub DEGs), as a receptor tyrosine kinase, was selected as a target for various drugs in lung cancer, such as Capmatinib, Tepotinib, Capmatinib, and Tepotinib, etc. Together, these findings explained the prognostic role and treatment implications of CMS in glioma at the molecular level (detailed discussion refer to Supplementary Discussion 1).

The tumor immune microenvironment plays an important role in tumor progression. In glioma, NK cells, macrophages, neutrophils, $CD4^+$ T cells, $CD8^+$ T cells, regulatory T cells, etc. influence disease outcome.[34] Molinaro et al[35] evaluated immune cell fractions and epigenetic age in glioma patients and found that IDH/1p19q/TERT-WT patients had lower lymphocyte fractions ($CD4^+$ T, $CD8^+$ T, NK, and B cells) and higher neutrophil fractions than people without glioma, suggesting that common host immune factors among different glioma types may affect survival. Consist with previous studies, we showed that T cells (including $CD4^+$ T cells, $CD8^+$ T cells, gamma delta T cells, regulatory T cells), B cells, plasma cells, macrophages, NK cells, neutrophils, mast cells, etc. were higher in subtype type 2 patients, suggesting higher immune infiltration in tumors of subtype 2 patients. Moreover, we examined expression levels of immune inhibitory receptor CTLA-4 and PD-1 and the ligand of PD-1 (ie, PDCD1L1), HAVCR2, LGALS9, CD86, LAG3, PDCD1LG2, CD28, CD96, CD80, and IDO1. The expression levels of these immune suppression molecules (Figure 6A, Supplementary Figure 16) were significantly or tend to be significantly higher in the poor-prognosis subtype.

CTLA-4 inhibits T-cell activation by inducing antigen-presenting cells to express CD80 and CD86.[36] Regulatory T cells can inhibit T-cell function by secreting IL-10 and TGF-β.[37] Studies have reported that neutrophil infiltration in tumor tissues can promote tumor progression and metastasis, and in glioma, neutrophils can promote tumor proliferation by inducing angiogenesis.[38–40] NK cells are an important component of the human immune system. However, Poli et al showed that NK cells are in a state of inactivation in glioma.[41] These results indicated possible mechanisms for immune escape or immune tolerance due to the influence of immunosuppressive cell (eg, regulatory T cells) infiltration, T-cell function inactivation, and other factors in the poor subtype tumors, which could explain the poor prognosis of subtype 2 patients in spite of more immune cells enriched in this subtype. Given the role of these immunosuppressive molecules in cancer immunotherapy, CMS also lays the foundation to select patients for the

targeted immunotherapy.[34] Surprisingly, there was no significant association between PIK3CA/PIK3R1 mutation or CDKN2A/B copy number alternation and CMBs (Supplementary Figures 18 and 19); also, no significant association between homologous recombination deficiency and CMS was identified (Supplementary Figure 20), despite their clinical value in gliomas.[42,43]

This study has some shortcomings. First, relatively few LGG patients were included in the validation cohorts, so the conclusions of this study need further verified in large-scale studies. Second, the prevalence of subtype 2 was potentially due to the differences in patient population across hospitals. Nevertheless, our findings demonstrated the robustness and significant clinical value of CMS in all five cohorts. However, further large-scale studies are still needed to evaluate the impact of population difference on CMS before its utility in clinical practice. Third, our findings raise the possibility that subtype 2 LGG patients could benefit from anti-PD-1 immunotherapy; however, since LGG patients have not been recommended for anti-PD-1 immunotherapy based on existing clinical practice, we could not find any retrospective dataset to test this and will investigate it in our future prospective study.

In conclusion, we developed a pathology image-based LGG subtyping that seems to stratify LGG patients into two groups with different OS associated with treatment responses, copy number alterations, and TMB levels and immune tolerance. It provides a cost-effective solution with potential applicability worldwide in current clinical settings (Supplementary Table 28).

Supplementary Material

Supplementary material is available at *Neuro-Oncology* online.

Keywords

cellular morphometric biomarkers | cellular morphometric subtypes | glioblastoma | immunohistochemistry | lower-grade glioma | nomogram | overall survival | stacked predictive sparse decomposition

Funding

This work was supported by the National Cancer Institute (NCI) at the National Institutes of Health (NIH) [R01CA184476 to H.C.]. Additional support was provided by Zhongnan Hospital of Wuhan University [ZLYNXM202011 to Z.Q.L.] for independent validation at Zhongnan Hospital. Lawrence Berkeley National Laboratory (LBNL) is a multi-program national laboratory operated by the University of California for the DOE under contract DE AC02-05CH11231.

Acknowledgments

We thank Dr. Lee A. Cooper for providing SCNN Risk Score for our independent evaluation and his thoughtful suggestions and Dr. Angus Martin Shaw Toland for his support on data collection at Stanford University.

Conflict of interest statement. The authors declare no conflicts of interest.

Authorship statement. Study design and funding acquisition: H.C. and Z.Q.L.; Validation cohort study: H.V. and Z.Q.L.; Data acquisition: X.J. and S.S.A.; Pathological interpretation: H.V., S.F.T., Y.X.C., and P.J.D.; Clinical interpretation: Z.Q.L. and W.A.W.; Statistical guidance: J.H.M.; Algorithm design and data analysis: H.C., X.P.L., and X.Y.; Data maintenance: K.C.; IHC staining and assessment: S.F.T. and Y.X.C. Result interpretation: Y.X., X.J., A.M.S., P.J.D., W.A.W., J.H.M., and H.C.; Manuscript writing: J.H.M., H.C., A.M.S., P.J.D., and W.A.W. All authors read and approved the manuscript.

Data Availability

TCGA-LGG and TCGA-GBM data are publicly available at GDC portal; Patient CMS and clinical data are available as supplementary materials; WSIs from ZN-GBM, ZN-LGG, and SU-LGG cohorts are available upon request to corresponding authors after IRB approval; Code for CMB detection and application with pre-trained SPSD model will be available upon request to corresponding authors.

References

1. Sidaway P. Low-grade glioma subtypes revealed. *Nat Rev Clin Oncol.* 2020;17:335.
2. Sturm D, Pfister SM, Jones DTW. Pediatric gliomas: current concepts on diagnosis, biology, and clinical management. *J Clin Oncol.* 2017;35:2370–2377.
3. Louis DN, Perry A, Wesseling P, Brat DJ, Cree IA, Figarella-Branger D, et al. The 2021 WHO Classification of Tumors of the Central Nervous System: a summary. *Neuro Oncol.* 2021;23:1231–1251.
4. Louis DN, Perry A, Reifenberger G, von Deimling A, Figarella-Branger D, Cavenee WK, et al. The 2016 World Health Organization Classification of Tumors of the Central Nervous System: a summary. *Acta Neuropathol.* 2016;131:803–820.
5. Keshri V, Deshpande RP, Chandrasekhar Y, Panigrahi M, Rao IS, Babu PP. Risk stratification in low grade glioma: a single institutional experience. *Neurol India.* 2020;68:803–812.
6. Viaccoz A, Lekoubou A, Ducray F. Chemotherapy in low-grade gliomas. *Curr Opin Oncol.* 2012;24:694–701.
7. Sharma A, Graber JJ. Overview of prognostic factors in adult gliomas. *Ann Palliat Med.* 2021;10:863–874.

8. Liang J, Lv X, Lu C, Ye X, Chen X, Fu J, et al. Prognostic factors of patients with gliomas—an analysis on 335 patients with glioblastoma and other forms of gliomas. *BMC Cancer.* 2020;20:35.
9. Ceccarelli M, Barthel FP, Malta TM, Sabedot TS, Salama SR, Murray BA, et al. Molecular profiling reveals biologically discrete subsets and pathways of progression in diffuse glioma. *Cell.* 2016;164:550–563.
10. Louis DN, Perry A, Reifenberger G, von Deimling A, Figarella-Branger D, Cavenee WK, et al. The 2016 World Health Organization Classification of Tumors of the Central Nervous System: a summary. *Acta Neuropathol.* 2016;131:803–820.
11. Özcan H, Emiroğlu BG, Sabuncuoğlu H, Özdoğan S, Soyer A, Saygı T. A comparative study for glioma classification using deep convolutional neural networks. *Math Biosci Eng.* 2021;18:1550–1572.
12. Ning Z, Luo J, Xiao Q, Cai L, Chen Y, Yu X, et al. Multi-modal magnetic resonance imaging-based grading analysis for gliomas by integrating radiomics and deep features. *Ann Transl Med.* 2021;9:298.
13. Fukuma R, Yanagisawa T, Kinoshita M, Shinozaki T, Arita H, Kawaguchi A, et al. Prediction of IDH and TERT promoter mutations in low-grade glioma from magnetic resonance images using a convolutional neural network. *Sci Rep.* 2019;9:20311.
14. Chang H, Han J, AD B, Loss L, Gray J, Spellman P, et al. Invariant delineation of nuclear architecture in glioblastoma multiforme for clinical and molecular association. *IEEE Trans Med Imaging.* 2013;32:670–682.
15. Chang H, Borowsky A, Spellman P, Parvin B. Classification of tumor histology via morphometric context. Paper presented at: 2013 IEEE Conference on Computer Vision and Pattern Recognition, Portland, OR, USA, June 23–28, 2013.
16. Chang H, Fontenay GV, Han J, Cong G, Baehner FL, Gray JW, et al. Morphometic analysis of TCGA glioblastoma multiforme. *BMC Bioinformatics.* 2011;12:484.
17. Chang H, Zhou Y, Borowsky A, Barner K, Spellman P, Parvin B. Stacked predictive sparse decomposition for classification of histology sections. *Int J Comput Vis.* 2015;113:3–18.
18. Wolchok JD, Hoos A, O'Day S, Weber JS, Hamid O, Lebbé C, et al. Guidelines for the evaluation of immune therapy activity in solid tumors: immune-related response criteria. *Clin Cancer Res.* 2009;15:7412–7420.
19. McKenna SJ, Ricketts IW, Cairns AY, Hussein KA. A comparison of neural network architectures for cervical cell classification. Paper presented at: 1993 Third International Conference on Artificial Neural Networks, Brighton, UK, May 25–27, 1993;105–109.
20. Charles NA, Holland EC, Gilbertson R, Glass R, Kettenmann H. The brain tumor microenvironment. *Glia.* 2011;59:1169–1180.
21. Zhou M. Restricted mean survival time and confidence intervals by empirical likelihood ratio. *J Biopharm Stat.* 2021;31:362–374.
22. Mobadersany P, Yousefi S, Amgad M, Gutman DA, Barnholtz-Sloan JS, Velázquez Vega JE, et al. Predicting cancer outcomes from histology and genomics using convolutional networks. *Proc Natl Acad Sci USA.* 2018;115:E2970.
23. Petralia F, Tignor N, Reva B, Koptyra M, Chowdhury S, Rykunov D, et al. Integrated proteogenomic characterization across major histological types of pediatric brain cancer. *Cell.* 2020;183:1962–1985.e31.
24. Marabelle A, Fakih M, Lopez J, Shah M, Shapira-Frommer R, Nakagawa K, et al. Association of tumour mutational burden with outcomes in patients with advanced solid tumours treated with pembrolizumab: prospective biomarker analysis of the multicohort, open-label, phase 2 KEYNOTE-158 study. *Lancet Oncol.* 2020;21:1353–1365.
25. Wang L, Ge J, Lan Y, Shi Y, Luo Y, Tan Y, et al. Tumor mutational burden is associated with poor outcomes in diffuse glioma. *BMC Cancer.* 2020;20:213.
26. Pal J, Patil V, Kumar A, Kaur K, Sarkar C, Somasundaram K. Genetic landscape of glioma reveals defective neuroactive ligand receptor interaction pathway as a poor prognosticator in glioblastoma patients [abstract]. Paper presented at: Proceedings of the American Association for Cancer Research Annual Meeting 2017; Washington, DC; April 1–5. Philadelphia (PA): AACR; 2017.
27. Nijaguna MB, Patil V, Hegde AS, Chandramouli BA, Arivazhagan A, Santosh V, et al. An eighteen serum cytokine signature for discriminating glioma from normal healthy individuals. *PLoS One.* 2015;10:e0137524.
28. Wang B, Zhao CH, Sun G, Zhang ZW, Qian BM, Zhu YF, et al. IL-17 induces the proliferation and migration of glioma cells through the activation of PI3K/Akt1/NF-kappaB-p65. *Cancer Lett.* 2019;447:93–104.
29. Parajuli P, Mittal S. Role of IL-17 in glioma progression. *J Spine Neurosurg.* 2013;Suppl 1:pii:S1-004.
30. Yarmoska SK, Alawieh AM, Tomlinson S, Hoang KB. Modulation of the complement system by neoplastic disease of the central nervous system. *Front Immunol.* 2021;12:689435.
31. Shan Y, He X, Song W, Han D, Niu J, Wang J. Role of IL-6 in the invasiveness and prognosis of glioma. *Int J Clin Exp Med.* 2015;8:9114–9120.
32. Yang F, He Z, Duan H, Zhang D, Li J, Yang H, et al. Synergistic immunotherapy of glioblastoma by dual targeting of IL-6 and CD40. *Nat Commun.* 2021;12:3424.
33. Hibi M, Murakami M, Saito M, Hirano T, Taga T, Kishimoto T. Molecular cloning and expression of an IL-6 signal transducer, gp130. *Cell.* 1990;63:1149–1157.
34. Qi Y, Liu B, Sun Q, Xiong X, Chen Q. Immune checkpoint targeted therapy in glioma: status and hopes. *Front Immunol.* 2020;11:578877.
35. Molinaro AM, Wiencke JK, Warrier G, Koestler DC, Chunduru P, Lee JY, et al. Interactions of age and blood immune factors and non-invasive prediction of glioma survival. *J Natl Cancer Inst.* 2021;114:446–457.
36. Fong B, Jin R, Wang X, Safaee M, Lisiero DN, Yang I, et al. Monitoring of regulatory T cell frequencies and expression of CTLA-4 on T cells, before and after DC vaccination, can predict survival in GBM patients. *PLoS One.* 2012;7:e32614.
37. Bettelli E, Carrier Y, Gao W, Korn T, Strom TB, Oukka M, et al. Reciprocal developmental pathways for the generation of pathogenic effector TH17 and regulatory T cells. *Nature.* 2006;441:235–238.
38. Khan S, Mittal S, McGee K, Alfaro-Munoz KD, Majd N, Balasubramaniyan V, et al. Role of neutrophils and myeloid-derived suppressor cells in glioma progression and treatment resistance. *Int J Mol Sci.* 2020;21:1954.
39. Garrido-Navas C, de Miguel-Perez D, Exposito-Hernandez J, Bayarri C, Amezcua V, Ortigosa A, et al. Cooperative and escaping mechanisms between circulating tumor cells and blood constituents. *Cells.* 2019;8:1382.
40. Fujita M, Scheurer ME, Decker SA, McDonald HA, Kohanbash G, Kastenhuber ER, et al. Role of type 1 IFNs in antiglioma immunosurveillance—using mouse studies to guide examination of novel prognostic markers in humans. *Clin Cancer Res.* 2010;16:3409–3419.
41. Poli A, Wang J, Domingues O, Planaguma J, Yan T, Rygh CB, et al. Targeting glioblastoma with NK cells and mAb against NG2/CSPG4 prolongs animal survival. *Oncotarget.* 2013;4:1527–1546.
42. Draaisma K, Wijnenga MMJ, Weenink B, Gao Y, Smid M, Robe P, et al. PI3 kinase mutations and mutational load as poor prognostic markers in diffuse glioma patients. *Acta Neuropathol Commun.* 2015;3:88.
43. Lu VM, O'Connor KP, Shah AH, Eichberg DG, Luther EM, Komotar RJ, et al. The prognostic significance of CDKN2A homozygous deletion in IDH-mutant lower-grade glioma and glioblastoma: a systematic review of the contemporary literature. *J Neurooncol.* 2020;148:221–229.